ISSN 0020-4412, Instruments and Experimental Techniques, 2011, Vol. 54, No. 1, pp. 92–96. © Pleiades Publishing, Ltd., 2011.
Original Russian Text © A.Yu. Semanin, G.D. Sokolov, A.M. Tikhonov, 2011, published in Pribory i Tekhnika Eksperimenta, 2011, No. 1, pp. 100–104.

ELECTRONICS AND RADIO ENGINEERING

A Wideband Spectrometer for NMR Studies

A. Yu. Semanin[a,b], G. D. Sokolov[a,b], and A. M. Tikhonov[a]*

[a] *Kapitza Institute for Physical Problems, Russian Academy of Sciences, ul. Kosygina 2, Moscow, 119334 Russia*
**e-mail: tikhonov@kapitza.ras.ru*
[b] *Moscow Institute of Physics and Technology, Institutskii per. 9, Dolgoprudnyi, Moscow oblast, 141700 Russia*

Received July 30, 2010

Abstract—The design of a wideband decimeter-wave (200–900 MHz) spectrometer with a magnetic induction of up to ~10 T is described. This spectrometer is intended for studying electronic–nuclear oscillations in antiferromagnets at low temperatures (4.2–1.3 K). Critical field $H_c = 2.5 \pm 0.3$ T of a reorientation transition in a noncollinear antiferromagnet $Mn_3Al_2Ge_3O_{12}$ at temperature $T \approx 1.3$ K was determined from a $^{55}Mn^{2+}$ NMR spectrum.

DOI: 10.1134/S0020441211010088

The special feature of resonance properties of antiferromagnets with $^{55}Mn^{2+}$ magnetic ions (100% isotopic composition) at temperatures $T \sim 1$ K consists in the correlation of nuclear oscillations with oscillations of the electronic system, which leads to a strong frequency–field dependence of the NMR spectrum or to the dynamic shift of its frequency [1–3]. In easy-plane antiferromagnets with a linear (over the field) mode of the antiferromagnetic resonance (e.g., $MnCO_3$), the dynamic shift of the NMR frequency is observed in magnetic fields up to $H \approx 0.5$ T [4]. In noncollinear antiferromagnets (e.g., $CsMnBr_3$), electronic and nuclear oscillations interact in a wider magnetic field range (~4 T) [5, 6].

The NMR spectrum of magnetic ions contains information on the structure of the ground state of an antiferromagnet, phase transitions in it, and its low-frequency spin dynamics [7]. The frequency band, in which the NMR spectrum is usually recorded, is 200–700 MHz. A high resonance frequency ($\gamma_n H_n \sim 600$–700 MHz) in magnetically ordered materials with Mn^{2+} ions is caused by an enormous average local field at a nucleus ($H_n \sim 60$ T), which is basically determined by hyperfine interaction of nuclear and ion spins (gyromagnetic ratio $\gamma_n \approx 10.6$ MHz/T for ^{55}Mn). The NMR signal intensity is mainly determined by the effect of amplification of the radio-frequency (RF) field by the transverse component of the hyperfine field [8], making it possible to observe NMR signals when the external radio-frequency field is polarized $\mathbf{h} \parallel \mathbf{H}$ [9, 10].

To satisfy the wideband measurement requirements, it is convenient to use a continuous NMR circuit with a high-Q tunable cavity [11]. In this work, we describe the design of the decimeter-wave (wavelength λ varies from 30 to 100 cm) spectrometer, which is the upgraded version of the instrument described in [5, 6]. The analog automatic frequency control (AFC) system of the old spectrometer has been replaced with the digital AFC system, and a fundamentally new cavity is used.

A broadbandness of the spectrometer is, first of all, ensured by two types of tunable resonance systems. The first system is based on the earlier designed modification of the split-ring cavity [12]. Its design is sketched in Fig. 1. The cavity housing in Fig. 1a is a $10 \times 30 \times 8$ mm parallelepiped ($8 \times 20 \times 11$ mm parallelepiped in Fig. 1b), which is made of oxygen-free copper. In the split ring, the inductance is an 8-mm-diameter through hole, and the capacitance is a narrow slot (the gap is ~0.1 mm wide) in the cavity housing. The slot length L_0 specifies the cavity's eigenfrequency ν_0, since $\nu_0 \sim L_0^{-1/2}$.

The spectrometer frequency is tuned in a ~200- to 900-MHz band using three split rings with various geometries of slot *1*, into which mica plates with a 50- to 100-μm thickness are placed to finely tune the eigenfrequency (see Fig. 2). By shifting copper plate *2*, it is possible to change the capacitance between the plate and cavity *3* (isolator *4* is a 5- to 10-μm-thick polyethylene terephthalate film), which is used to tune the resonance frequency of the system. The RF power is supplied via coaxial line *5*. The inductive coupling with the cavity is affected by means of coupling loops, one of which is transmitting loop *6* and the other is receiving loop *7*. The ~5-mm-diameter coupling loops are placed at a ~5-mm distance from the faces of the cavity (weak coupling). The loaded Q factor of the resonance system in the band under investigation depends on the frequency and varies from 200 to 400 at the liquid helium temperature. Depending on the orientation of the cavity axis with respect to the magnetic field **H** (see Fig. 1), it is possible to perform

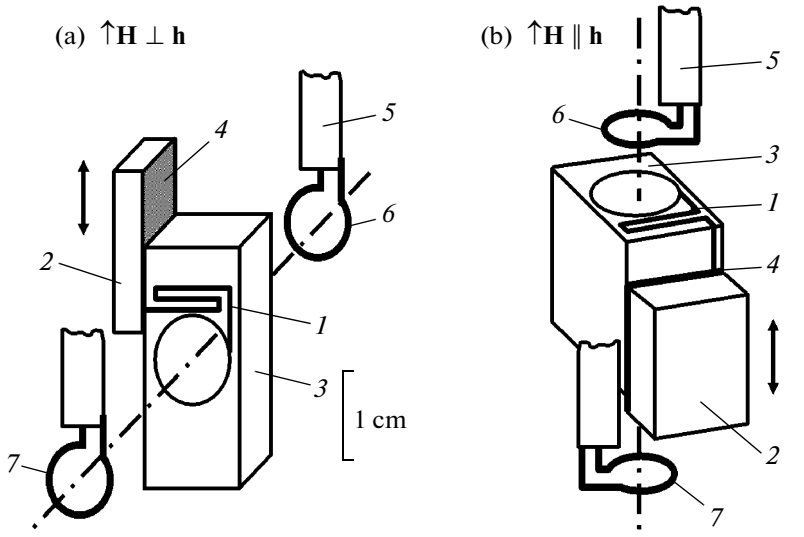

Fig. 1. Polarization of the RF field in the split-ring resonance system: (*1*) narrow slot, (*2*) copper plate, (*3*) cavity, (*4*) polyethylene terephthalate film, (*5*) coaxial line, and (*6, 7*) coupling loops.

experiments at two polarizations of RF field **h**: (a) **h** ⊥ **H** and (b) **h** ∥ **H**.

In contrast to the first system, the second-type resonance system features a significantly higher Q (~3000, see Fig. 3). It is based on a closed cavity, which is a shorted coaxial line 100 mm long (~λ/4). The coaxial cavity consists of copper cylinder *1* (20-mm inner diameter), copper core *2* (8-mm diameter), and bronze membrane *3* with a 0.2-mm thickness. Three is a narrow gap (0.2–0.5 mm) between the core and membrane. Its value can be changed by exerting pressure on the membrane using rod *4*. The cavity is coupled by coaxial lines *5* through 2-mm-diameter holes in the cylinder wall.

The lines of the RF magnetic field in the coaxial resonator are the concentric circumferences with a center lying on the axis of the cavity. The amplitude of this field assumes the minimal value on the membrane and the maximal value on the lower wall of the cavity. Flat coupling loops *6* are oriented in a radial direction at right angle to force lines of the RF magnetic field in the upper part of the cavity, where its amplitude is small, and a sufficiently weak coupling can be arranged.

The external magnetic field is applied along the axis of the cavity. Crystal sample *7* is placed at the bottom of the cavity at a maximum of the RF and stationary magnetic field (**h** ⊥ **H**), which is created by superconducting solenoid *8* (with an 80-mm outer diameter and 25-mm inner diameter). The critical current of the solenoid is ~67 A at a ~9.7-T maximal induction. The intensity of the magnetic field in the experiment is determined from the current produced by the bipolar power source (Cryomagnetics-4G-100). The calculated field inhomogeneity in the center of the solenoid is ±0.1% in 1 cm^3.

The entire assembly is in a helium bath (glass Dewar flask with a 90-mm inner diameter). Its temperature is controlled by a ^{4}He equilibrium saturated vapor pressure regulator with an accuracy of ±0.05 K or better.

At the liquid helium temperature, the eigenfrequency of the system with the coaxial cavity can vary from ~600 to 625 MHz, and ν_0 of the split-ring system with the cavity shown in Fig. 2a can be tuned in a ~900- to 500-MHz band.

When the magnetic field increases to maximal values, the frequency stability of the first-type resonance system is ~0.1 MHz, while the second resonance system allows one to fix the frequency in the experiment with a ~10-kHz accuracy. This is likely to be attributed to a high mechanical rigidity of the coaxial cavity.

A block diagram of the spectrometer is shown in Fig. 4. The frequency of the RF signal generator *G* (Agilent N9310A) is modulated by a low frequency (f_m = 25 kHz) of the auxiliary generator of the phase-sensitive voltmeter V_1 (SR 830 lock-in amplifier). The frequency modulation depth of 0.1 MHz (the maximal frequency deviation resolved by the generator) is significantly smaller than the typical NMR line width, which is usually >1 MHz. To stabilize the generator frequency on the top of the resonance peak, the AFC system tuned to zero amplitude of the first modulation harmonic is used. The AFC system includes a synchronous detector and digital tracking system operating in the LabView graphic programming environment (National Instruments). When the generator frequency is detuned from the eigenfrequency of the

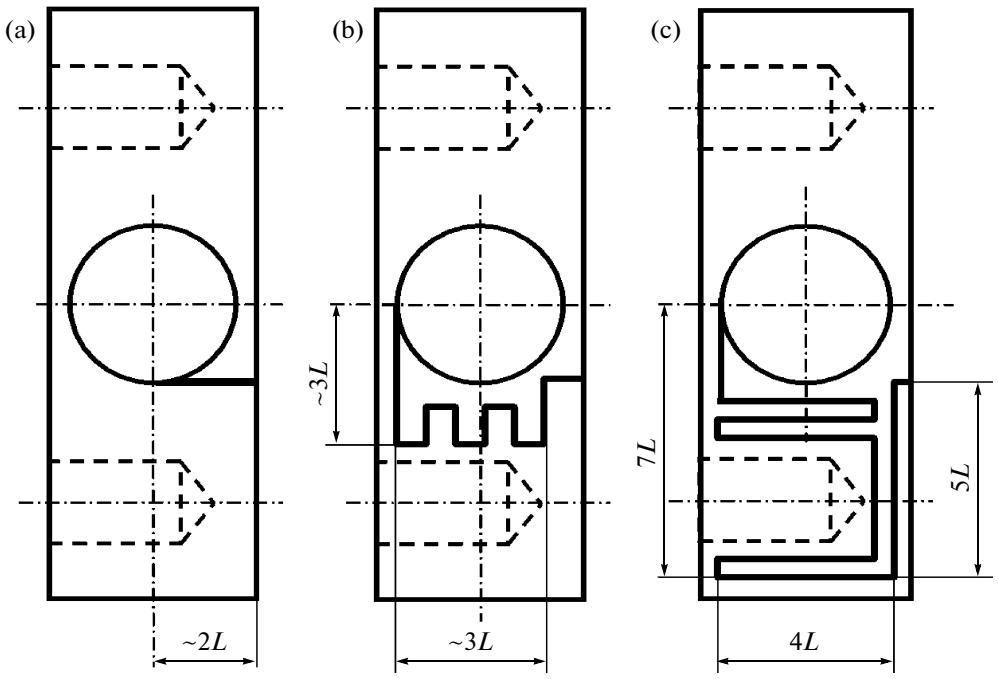

Fig. 2. Geometric parameters of slots in the split-ring cavities (polarization $\mathbf{h} \perp \mathbf{H}$) with eigenfrequency ν_0: (a) ~900, (b) ~450, and (c) ~250 MHz. The through hole diameter is 8 mm, $L = 2$ mm.

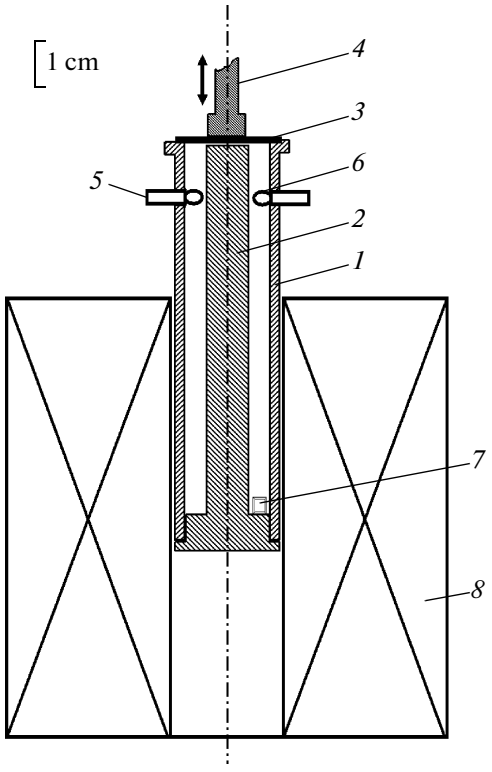

Fig. 3. Low-temperature part of the NMR spectrometer with a coaxial cavity: (*1*) cavity walls, (*2*) core, (*3*) membrane, (*4*) rod, (*5*) coaxial line, (*6*) coupling loop, (*7*) sample, and (*8*) solenoid.

cavity, signal U_f appears on detector D (planar diode) at the modulation frequency (first harmonic) with the phase depending on a mismatch sign. The amplitude of this signal detected by phase-sensitive voltmeter V_1 is, as a first approximation, proportional to the mismatch value between the generator frequency and the eigenfrequency of the resonance system (*RS*). The digital tracking system uses the detected mismatch signal for calculating correction $d\Omega$ to the carrier frequency of the RF signal generator as follows:

$$d\Omega = \alpha P\left(U_f + I\int_0^t U_f dt + D\frac{dU_f}{dt}\right), \qquad (1)$$

where P, I, and D are the feedback characteristics dependent on temperature, Q, and other factors. Their values are selected manually; usually, $P \gg I, D$. Constant α is determined by the second derivative value of the amplitude–frequency characteristic of the system on the top of the resonance peak.

To smooth the amplitude–frequency characteristic of the supplying high-frequency section, decoupling attenuators *At1* (10 dB) and *At2* (3 dB) are placed at the input and output of the low-temperature part of the spectrometer. The output power of the RF generator is 0.1 W. The absorption in the resonance section is detected by the second phase-sensitive voltmeter V_2 (SR 830 lock-in amplifier) from variations of the second harmonic signal amplitude U_{2f}.

The spectrometer is intended to perform measurements in two modes: by scanning the magnetic field at

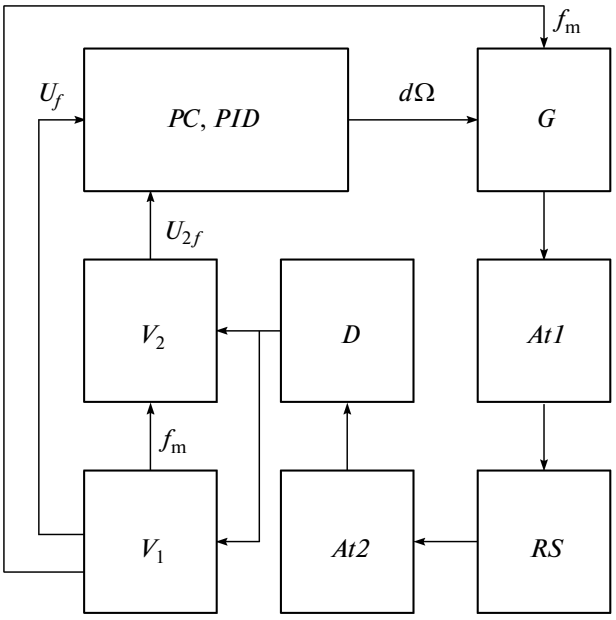

Fig. 4. Block diagram of the spectrometer. All devices are integrated into a common control system in the LabView graphic programming environment (National Instruments): (*RS*) resonance system, (*G*) RF signal generator, (*D*)planar diode, (V_1, V_2) phase-sensitive voltmeters, (*At1*, *At2*) attenuators, (*PC*) personal computer, (*PID*) feedback regulator calculating correction value $d\Omega$ to the generator carrier, (f_m) modulation signal, (U_f) signal of the first harmonic, and (U_{2f}) signal of the second harmonic.

a fixed generator frequency and by scanning the frequency at a fixed magnetic field. The need in this mode is caused by a weak dependence of the NMR frequencies on the field when the dynamic frequency shift is absent. Unfortunately, due to a low operation speed of the digital AFC (~10 Hz), we failed to use in full this operation mode of the spectrometer.

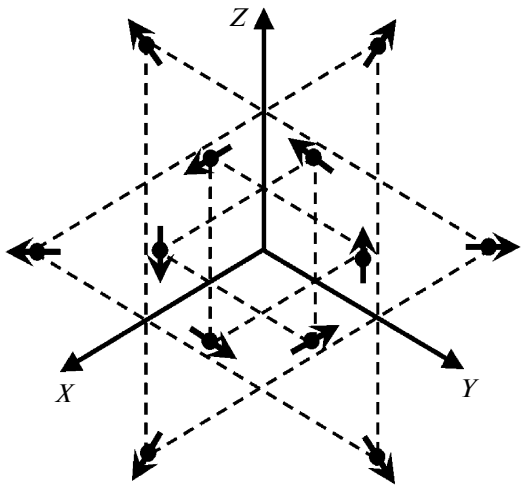

Fig. 5. Magnetic structure of noncollinear antiferromagnet $Mn_3Al_2Ge_3O_{12}$.

By using the spectrometer, we studied the reorientation phase transition in a cubic crystal (O_h^{10}) of manganese garnet $Mn_3Al_2Ge_3O_{12}$, which is the noncollinear 12-sublattice antiferromagnet with Néel temperature $T_N = 6.8$ K (see Fig. 5). According to neutron diffraction studies, Mn^{2+} magnetic moments in magnetically ordered states are located in plane (111), being aligned with axes [211], [121], and [112] or opposite to them. Thus, we obtain the noncollinear triangular 12-sublattice antiferromagnet ordering [13]. If the magnetic field is applied along direction [001], the spin plane rotates so that, in fields $H_c \gtrsim 3$ T, it is oriented perpendicularly to the field.

Figure 6 shows records of NMR spectra $\mathbf{h} \perp \mathbf{H}$ in the single crystal $Mn_3Al_2Ge_3O_{12}$ at $T \approx 1.3$ K, $\mathbf{H} \parallel$ [001], and (*1*) 604.4 MHz (the coaxial resonance system), and (*2*) 472.3 MHz (the split-ring resonance system). In all the scans, one can observe the minimum at $H_c = 2.5 \pm 0.3$ T, corresponding to the field of the phase transition. The appearance of the wide (in frequency) absorption line is obviously caused by interaction with a low-frequency branch of the antiferromagnetic resonance [14]. The value of the critical field H_c of the reorientation transition at $T \approx 1.3$ K is in agreement with magnetization measurement data in [15]. In scan *2*, the absorption in the vicinity of $H \approx 0$ is observed at frequencies below 600 MHz and demonstrates a strong hysteresis behavior. It apparently indicates that antiferromagnetic domains inside the sample disappear. In our future experiments, we plan

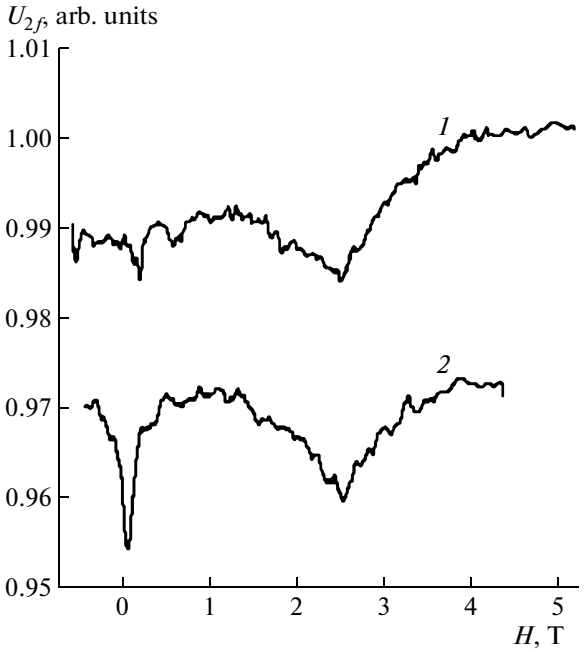

Fig. 6. Examples of NMR spectrum records at $\mathbf{h} \perp \mathbf{H}$ in single crystal $Mn_3Al_2Ge_3O_{12}$ at ≈1.3 K and $\mathbf{H} \parallel$ [001]: (*1*) 604.4 MHz, coaxial resonance system and (*2*) 472.3 MHz, split-ring resonance system.

to obtain more detailed information about evolution of the magnetic structure and low-frequency spin dynamics of $Mn_3Al_2Ge_3O_{12}$ in the magnetic field.

ACKNOWLEDGMENTS

We are grateful to B.V. Mil' for granting the manganese garnet single crystal and to A.I. Kleev and V.I. Marchenko for the useful discussions.

This work was supported in part by the Russian Foundation for Basic Research, project no. 090212341.

REFERENCES

1. De Gennes, P.G., Pincus, P., Hartmann-Bourtron, F., and Winter, J.M., *Phys. Rev.*, 1963, vol. 129, p. 1105.
2. Turov, E.A. and Petrov, M.P., *Ya.M.R. v ferro- i antiferromagnetikakh* (NMR in Ferro- and Antiferromagnets), Moscow: Nauka, 1969.
3. Kurkin, M.I. and Turov, E.A., *Ya.M.R. v magnitouporyadochennykh veshchestvakh i ego primenenie* (NMR in Magnetically Ordered Materials and its Application), Moscow: Nauka, 1990.
4. Borovik-Romanov, A.S. and Tulin, V.A., *Pis'ma Zh. Eks. Teor. Fiz.*, 1965, vol. 1/5, p. 18.
5. Borovik–Romanov, A.S., Petrov, S.V., Tikhonov, A.M., and Dumesh, B.S., *Zh. Eks. Teor. Fiz.*, 1998, vol. 86, p. 197.
6. Tikhonov, A.M., *Cand. Sci. (Phys.-Math.) Dissertation*, Moscow, Inst. for Physical Problems, Russ. Acad. of Sci., 1998.
7. Marchenko, V.I. and Tikhonov, A.M., *Pis'ma Zh. Eks. Teor. Fiz.,* 1999, vol. 69, p. 41.
8. Borovik–Romanov, A.S., Bun'kov, Yu.M., and Dumesh, B.S., *Usp. Fiz. Nauk*, 1984, vol. 27, p. 235.
9. Dumesh, B.S., Kurkin, M.I., Petrov, S.V., and Tikhonov, A.M., *Zh. Eks. Teor. Fiz.*, 1999, vol. 88, p. 1221.
10. Tikhonov, A.M. and Petrov, S.V., *Phys. Rev. B*, 2000, vol. 61, p. 9629.
11. Dumesh, B.S., *Prib. Tekh. Eksp.*, 1986, no. 1, p. 136.
12. Hardy, W.N. and Whitehead, L.D., *Rev. Sci. Instrum.,* 1981, vol. 52, p. 213.
13. Prandl, *Phys. Stat. Sol. B*, 1973, vol. 55, p. K159.
14. Prozorova, L.A., Marchenko, V.I., and Krasnyak, Yu.V., *Pis'ma Zh. Eks. Teor. Fiz.*, 1985, vol. 41, p. 522.
15. Kazei, Z.A., Kolmakova, N.P., Levanidov, M.V., et al., *Zh. Eks. Teor. Fiz.*, 1987, vol. 92, p. 2277.